Electronic Supplementary Material (ESI) for Journal of Materials Chemistry C.
This journal is © The Royal Society of Chemistry 2018

Supporting Information

Programmable and biomimetic photo-actuator: a composite of photo-liquefiable azobenzene derivative and commercial plastic film

*Jing Hu, Xiao Li, Yue Ni, Shudeng Ma and Haifeng Yu**

* Department of Material Science and Engineering, College of Engineering, and Key Laboratory of Polymer Chemistry and Physics of Ministry of Education, Peking University, Beijing 100871, China

* Email: yuhaifeng@pku.edu.cn

1. Supplementary Tables

Table S1. Phase transition temperatures[a)] of the photo-liquefiable azobenzene (PLAZ) derivative used in this study.

Molecule	**Phase transition temperature [°C]** [b)]		
	Isomer	Heating	Cooling
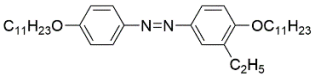	*trans*	Cr 62 I	I 44 N 40 Cr
	trans&*cis*[c)]	Cr_I 1.9 Cr_{II} 6.4 I	——[d)]

[a)] Obtained with DSC at a scan rate of 10 K min^{-1}; [b)] Cr: Crystal phase. N: nematic liquid crystal phase. I: isotropic liquid phase. Subscripts (I and II) indicate polymorphism; [c)] The PLAZ derivative were illuminated by 365 nm UV light for 10 min, and quenched in liquid nitrogen. [d)] The cooling transition temperature wasn't given for that the *cis* ratio was changing and different from the heating process.

2. Supplementary Schemes

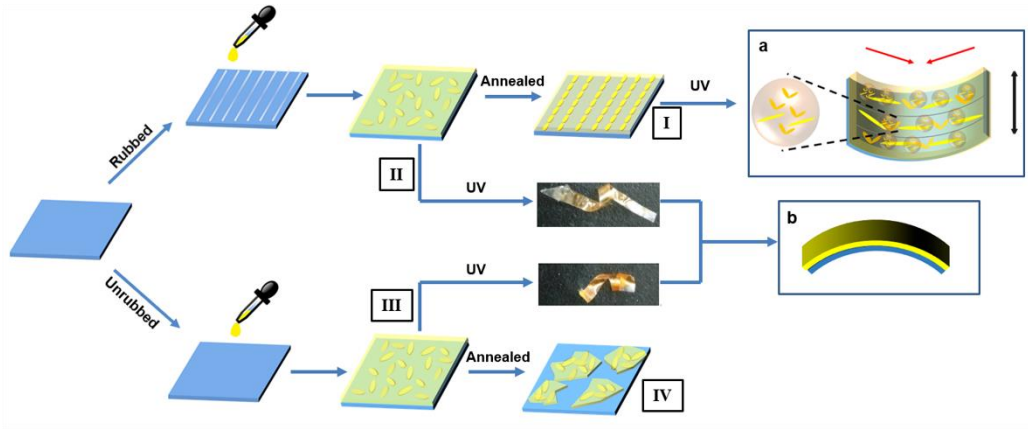

Scheme S1. The fabrication routes of the bilayer films (**I**, **II**, **III**, and **IV**) and the photomechanical response. a) The well-oriented bialyer actuator only bent towards the azo layer reversibly. The possible mechanism of photomechanical deformation of the bilayer film was given. The red arrows represent the contraction force, and the black arrow shows the expansion force. The black dash lines show the magnified picture of the liquid drop. The yellow rods represent the *trans*-azo molecules and orange bent rods represent the *cis*-azo molecules. b) The actuators without thermal annealing only bent towards the LDPE layer irreversibly.

Details about Scheme S1:

1. The photothermal effect and the plausible photo-actuated mechanism of composite films (II, III, and IV)

Since a majority of experiments were carried out with the UV light intensity higher than 100 mW/cm^2, the photothermal effect of the azobenzene chromophores should be taken into account (Fig. S12). The temperature elevation caused by the PLAZ derivative may act on the LDPE layer. The PLAZ derivatives in the bilayer actuator **II** and **III** were randomly distributed on the LDPE substrate (Figure S9a,b). The *trans*-to-*cis* photo-isomerization of the non-oriented PLAZ derivatives produce a volume expansion due to the free volume theory. [1-2] In addition, the LDPE film is a widely-used heat-shrinkable wrapping materials and may own a negative coefficient of thermal expansion (CTE) about -2×10^{-5}/K to -4×10^{-5}/K. [3] The semi-crystalline LDPE film (Figure S13) with a glass-transition temperature (Tg) far below zero Celcius degree [4] may also produce a contraction stress due to photothermal heat-shrinking. Consequently, the actuator **II** and **III** bended towards the LDPE layer. However, if the actuator **III** was annealed to become the actuator **IV**, no detectable photoinduced deformation was observed again. The reason is that the liquid azobenzene derivatives aggregated in the process of annealing and couldn't re-spread homogeneously on the LDPE surface for the absence of microgrooves. The dispersive sections of the PLAZ derivatives on LDPE substrate couldn't supply an integral expansion force nor efficient heater for heat-shrinkable LDPE film.

2. Reversibility of actuator **II**

Actuator **II** without annealing couldn't transform to actuator **I** after UV irradiation although a little amount of photoinduced liquid azobenzene may flow into the microgrooves and be oriented by the capillary force. The actuator **II** under UV irradiation is somewhat annealed. However, the namely photo-annealing (only lasting for several seconds) can't completely replace the thermal annealing (several hours). Photoirradiation caused the azobenzene to be isomerized into liquid. Only a little amount of liquid can be aligned along the microgrooves. As shown in Fig. S8d, the order parameter is still close to zero (0.03) after the photo-irradiation. Most of the PLAZ derivatives are still outside the microgrooves for the case of actuator **II**. As a result, the actuator **II** can't bend towards azobenzene layer like actuator **I** after the first photoresponsive circle.

3. Supplementary Figures

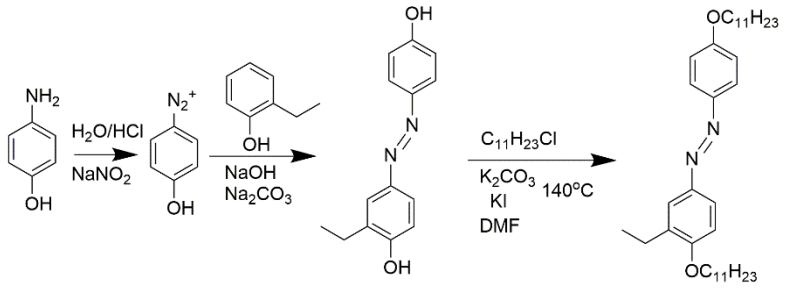

Fig. S1 The synthesis route of the PLAZ derivative (4,4'-diundecyloxy-3-ethylazobenzene).

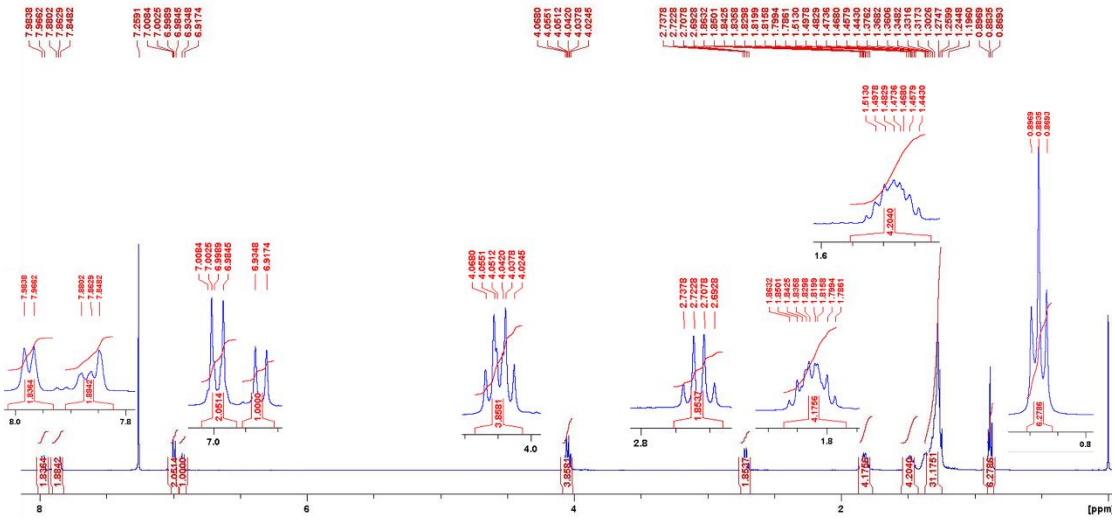

Fig. S2 ^{1}H NMR spectrum of the PLAZ derivative.

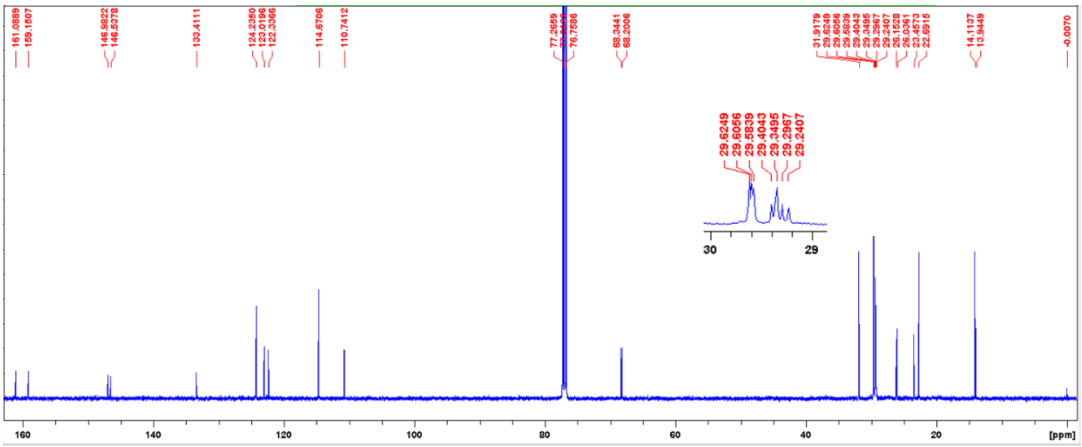

Fig. S3 ^{13}C NMR spectrum of the PLAZ derivative.

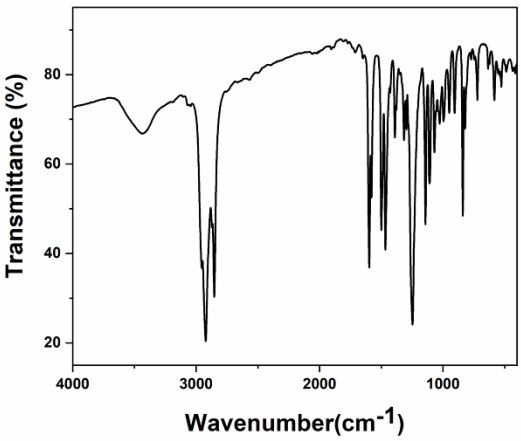

Wavenumber (cm^{-1})	Functional group
2922	$-CH_3$ (v_{as})
2853	$-CH_3$(v_s)
1499	N=N (v)
1466	-CH3 (β)
1247	Ar-O (v)
1142	C-C (v)
1108	Ar-O (v)
839	Para-Ar (v)

Fig. S4 FT-IR spectrum of the PLAZ derivative.

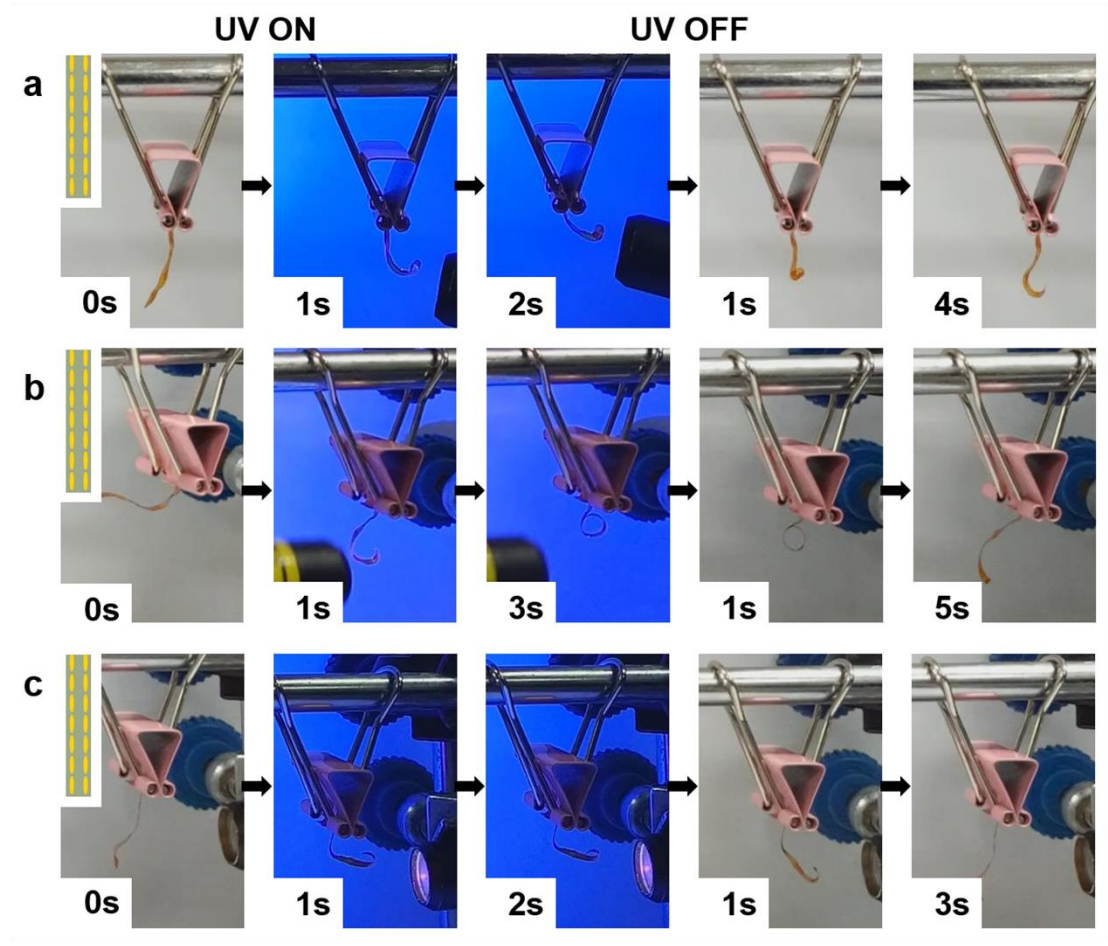

Fig. S5 Influence of light source on the photomechanical motions of the bilayer actuators **I**. a) The films were illuminated with 365 nm light from the azo layer side (>180 mW/cm^2). The light source was movable to supply enough light energy and appropriate illuminating position for efficient deformation. b) The film was illuminated with 365 nm light from the LDPE layer side (>180 mW/cm^2). The light source was movable too. c) The film was illuminated with 365 nm light from the azo layer (>180 mW/cm^2). The light source was fixed. As shown in the pictures, the strip in (a,b) can deform into a coil no matter with the light direction, while the strip in (c) can't deform into a coil. The insets at the upper left corner (the pictures at 0 s) represent the structure of bilayer films. Film size: 15 mm×3 mm×25 μm.

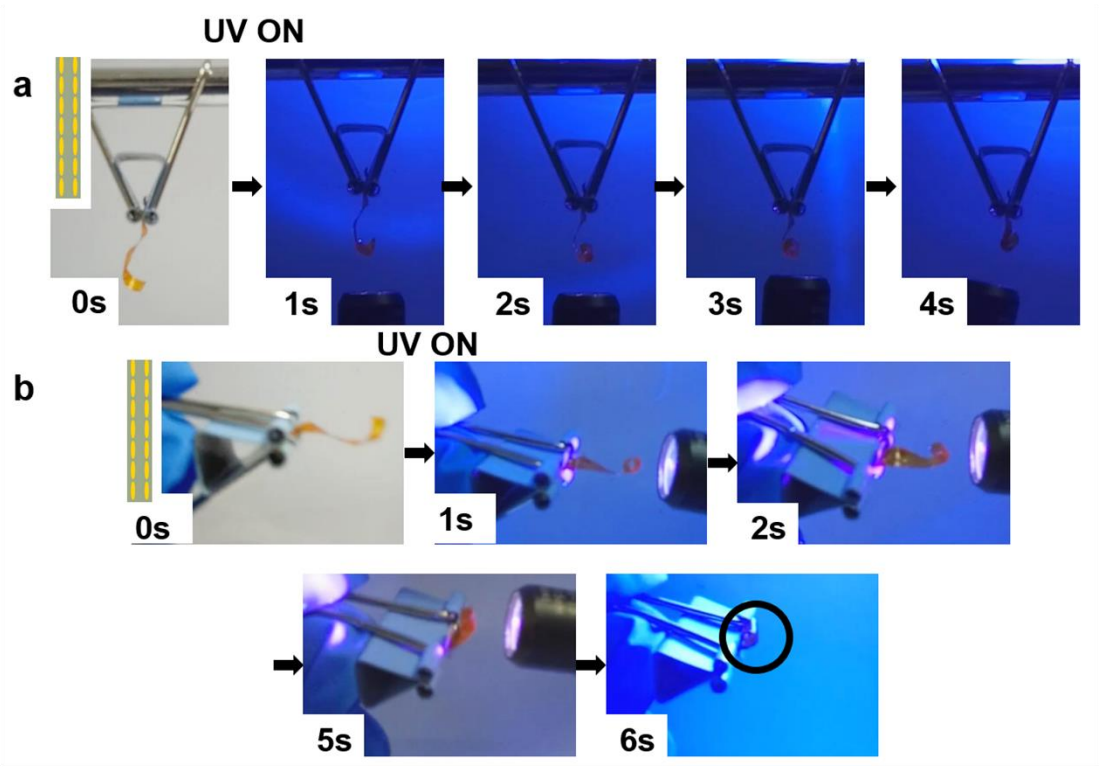

Fig. S6 Exclude the influence of gravity on the photomechanical deformation of the bilayer actuator **I**. a) The film was vertically illuminated with 365 nm light (>180 mW/cm^2). b) The film was transversely illuminated with 365 nm light (>180 mW/cm^2). The light source was movable. The black circle in the picture (6 s) showed the bilayer film. It strongly coiled into a multilayer roll. The insets at the upper left corner (pictures at 0 s) represent the structure of bilayer films. Film size: 15 mm×3 mm×25 μm.

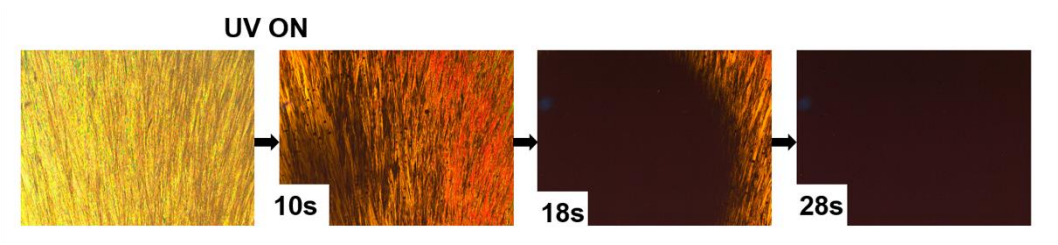

Fig. S7 Photoinduced phase transition of the PLAZ derivative at room temperature. The polarizing optical microscope (POM) images show the PLAZ derivative illuminated with 365 nm light (50 mW/cm^2). The sample (about 100 μm thick) was fabricated by melting the PLAZ derivative and then pressed between two pieces of quartz glass slides. The dark field after irradiation means the crystal transforming to isotropic liquid.

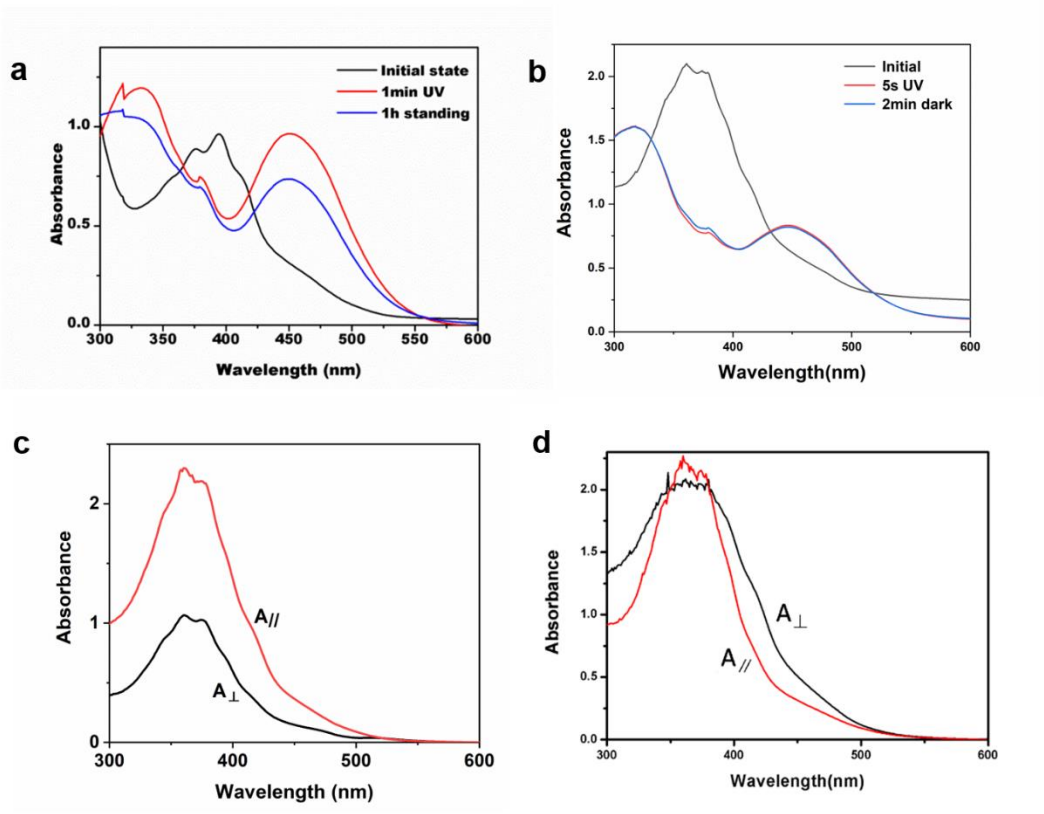

Fig. S8 a) The UV-vis absorption spectra of pure PLAZ derivative (thickness~100 μm). The sample was fabricated by melting the PLAZ derivative and then pressed it between two pieces of quartz glass slides. The *cis* content can be estimated by a formula: $(1-A/A_{trans})/(1-\varepsilon_{cis}/\varepsilon_{trans})$, where A is the absorbance of the composite film at 365 nm after UV irradiation, and ε_{cis} and ε_{trans} are the molar absorption coefficients of *cis* and *trans* isomers, $\varepsilon_{cis}/\varepsilon_{trans}$ is about 0.05.[5] The *cis* content in pure PLAZ derivative after 1 min UV light is about 42.1%. b) UV-vis absorption spectra of the bilayer actuator (azobenzene layer 10 μm). The photoisomerization takes a part in liquefying the PLAZ derivative. The intensity of UV light was 200 mW/cm^2. The *cis* content in actuator **I** after 5s UV is about 60.8%, and decreases to 58.5% after thermal back-isomerization. The difference between the spectra (a) and (b) is caused by the different thickness of the PLAZ derivative and the orientation of the PLAZ derivative. c) The polarized UV-vis absorption spectra of the bilayer film **I** after annealing. Here, // and ⊥ indicate the relationship between the orientation direction of the azo molecules and the direction of the polarized light. The order parameter, $S=(A_{par}-A_{per})/(A_{par}+2A_{per})=0.33$, where A_{par} and A_{per} are absorbance parallel and perpendicular to the rubbing direction. d) The polarized UV-vis absorption spectra of the bilayer film **II** after 20 s photo-irradiation and 24 h dark. The order parameter is close to zero (0.03).

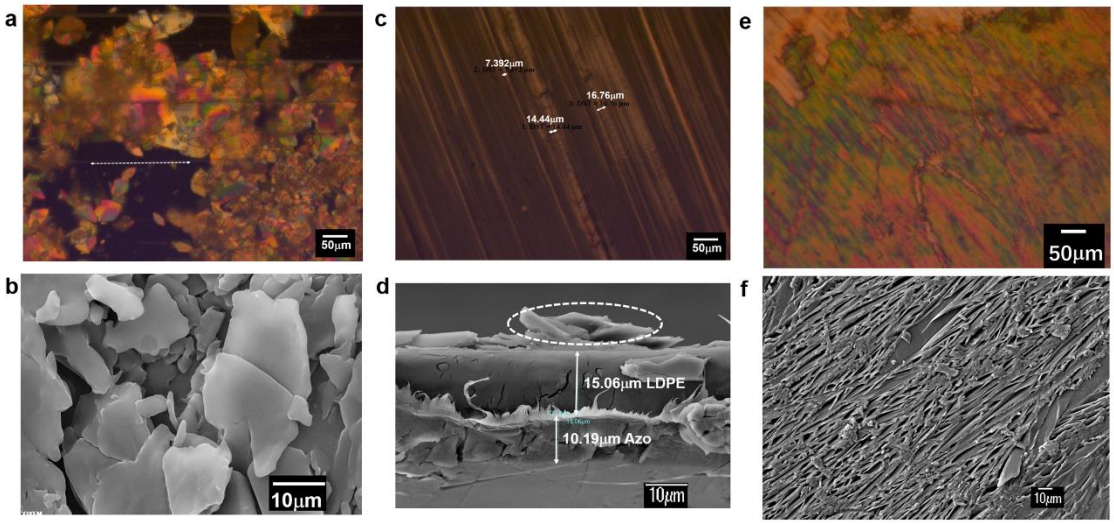

Fig. S9 Surface and cross-section morphology the of bilayer actuators. a) and b) are polarizing optical microscope (POM) and SEM images of the composite film **II**. The lamelliform PLAZ derivative lie on the LDPE substrate optionally. The dashed line in (a) shows the microgroove. c) POM image of the rubbed LDPE film. There is a distribution of the width and space between the microgrooves. d) SEM cross-section image of the composite film **I**. The dashed ellipse shows a little amount of non-oriented azo crystals. The total thickness of the bilayer actuator is about 25 μm. e) and f) are POM and SEM images of composite film **I**. The PLAZ derivative grow in a flaky texture along the microgrooves after annealing.

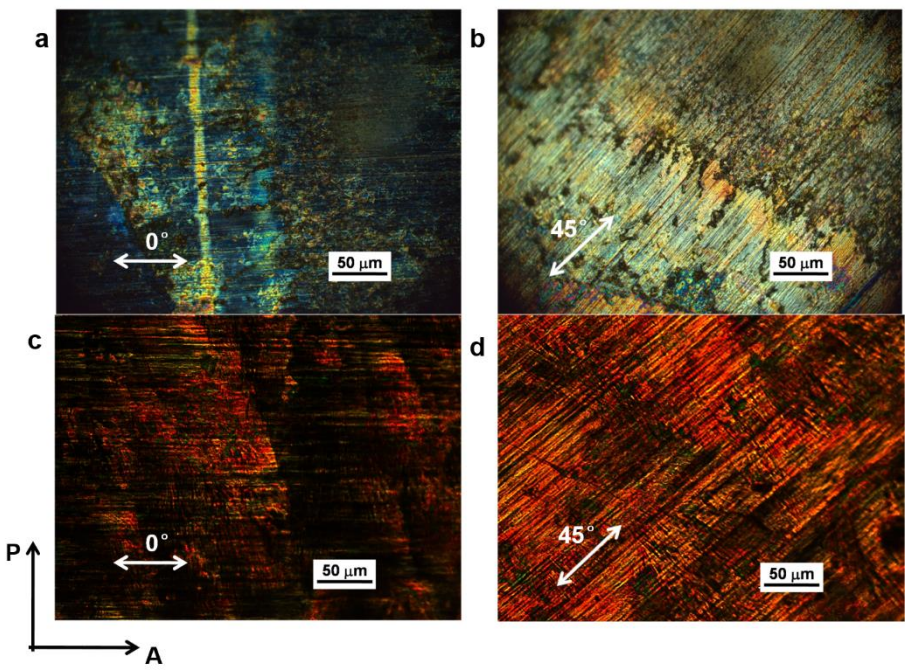

Fig. S10 Characterizations of the azo orientation in the bilayer film **I**. POM images of the bilayer films before (a,b) and after annealing (c,d). A: analyzer, P: polarizer. The double-sided arrow represents the rubbing direction. The values beside the arrows show the angle between the rubbing direction and the polarization direction of the analyzer. The periodic birefringence extinction proves the orientation of PLAZ derivatives along the microgrooves to some extent.

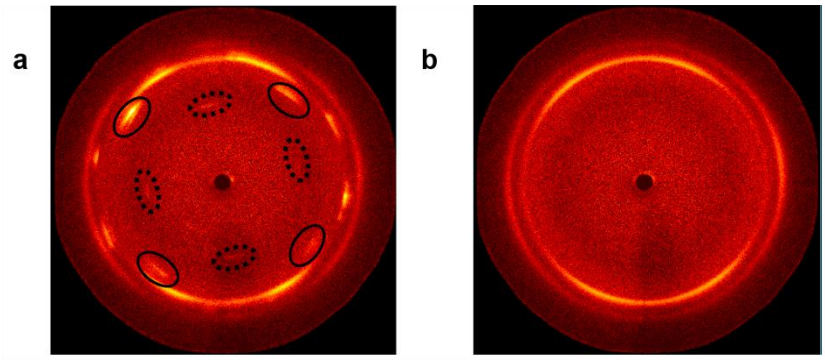

Fig. S11 a) The diffraction pattern of the bilayer film **I**. The solid and dotted ellipses demonstrate two groups of quadruple symmetric diffraction spots, which belongs to the PLAZ derivatives, can prove the orientation of PLAZ derivatives alonge the microgrooves. b) The double symmetric diffraction pattern of pure LDPE film. The crystalline part in LDPE film may be partially oriented to some extent due to the molding process.

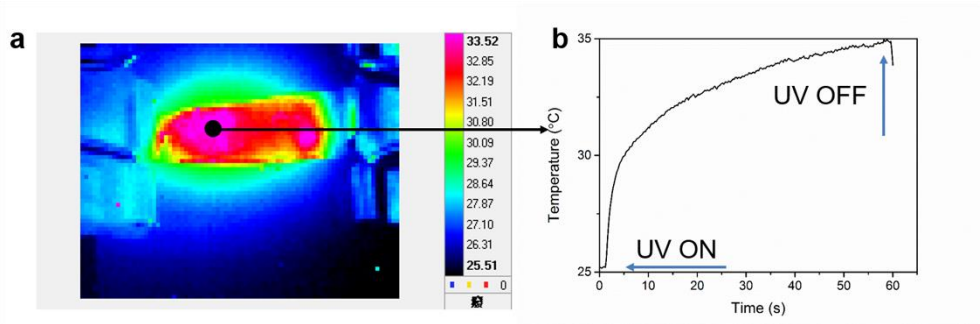

Fig. S12 Photothermal effect of the bilayer film upon irradiation of UV light. a) Infrared thermography of the bilayer film upon photoirradiation at a light intensity of 270 mW/cm^2 for 60 s. b) The temperature-time curve of a spot in the highest temperature region. A temperature elevation of 5°C was observed in 5 seconds, while 10°C within 60 seconds irradiation of UV light. The photothermal effect didn't action on the photo-liquefaction of the PLAZ derivative for the highest temperature (35°C) was still lower than the melting point of *trans* PLAZ derivative (The photo-isomerization is the main factor), but can action on the LDPE.

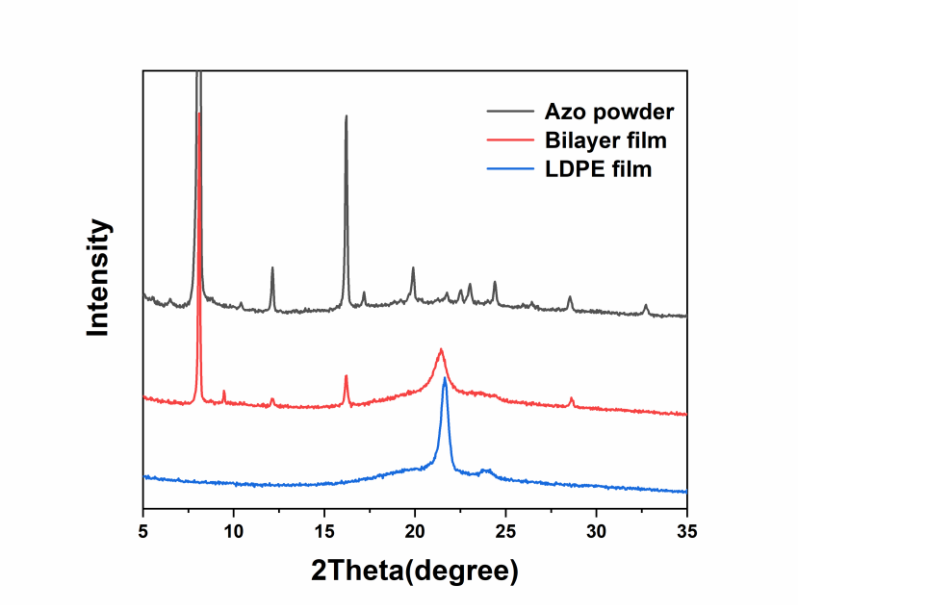

Fig. S13 X-ray diffraction spectra of the PLAZ derivative powder, LDPE substrate and the bilayer film. The peaks of bilayer film are a combination of the main peaks of the azo powder and LDPE film. The broad peak of LDPE film shows the semi-crystalline properties. Sharp peaks were observed in the XRD data of the azo powder, showing its better crystallization property, which were kept in the bilayer film.

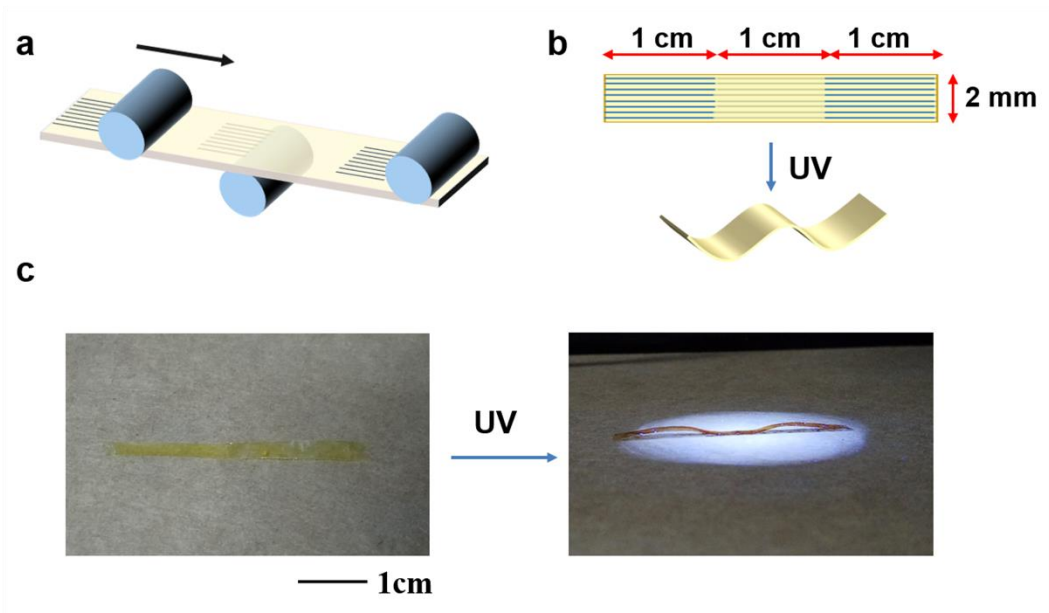

Fig. S14 Photodriven wave-shape deformation of the bilayer films. a) Scheme of rubbing LDPE substrate alternatively on its up and bottom surface (Black arrow shows the rubbing direction). b) Scheme of the strip structure and the deformation upon photoirradiation. Dark blue lines show the grooves on the upper surface and light blue lines show the grooves on the lower surface. (c) Photographs of real product upon irradiation of UV light (Thickness 27 μm, light intensity >100 mW/ cm^2).

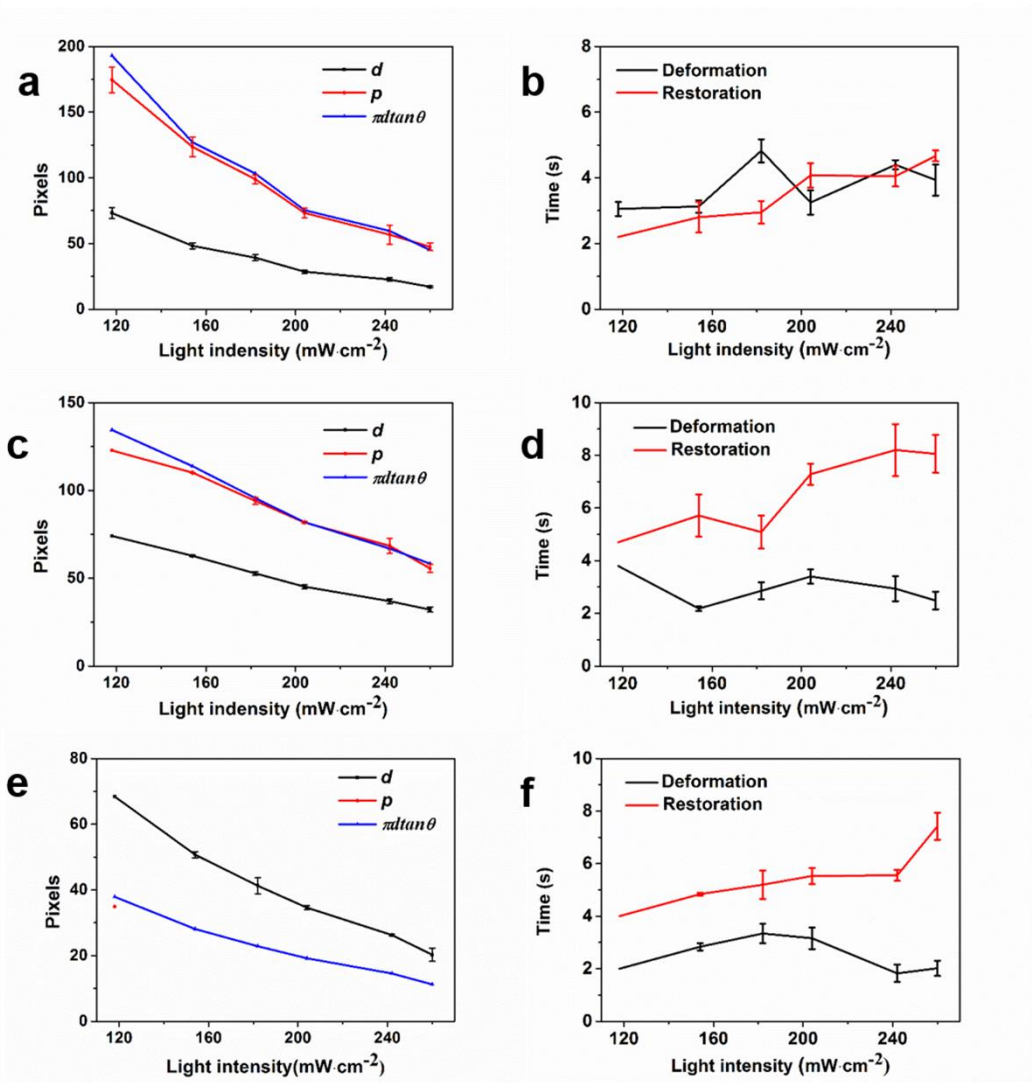

Fig. S15 Length change and response time of the bilayer film **I** upon photoirradiation at different light intensities. a) Pitch (p), diameter (d) and calculative pitch ($\pi d tan\theta$) of the right-handed helix film with θ_1 =40° upon photoirradiation of 365 nm light at different intensities. b) Deformation (under 365 nm light) and restoration (without illumination) time of the right-handed film with θ_1 =40°. c) and d) The left-handed helix film with θ_2 =30°. e) and f) The left-handed helix film with θ_2=10°. Only one measured pitch dot is given in e) because when $w/cos\theta$ (w is the width of strip) is bigger than the pitch, the circles of helix are overlapped and the pitch can't be measured exactly. Film size: 20 mm×3 mm×25 μm. The error bars give the deviation within four different measurements. Pixels are measured by the screenshots of the helical deformation movies, and are equivalent to the length unit. (b, d, f) The light intensity isn't the only determinant of deformation time and restoration time. The restoration time is somewhat depending on deformation amplitude. The response time may be an intrinsic parameter of the bilayer system which can be further investigated by changing the substrate and functional coating.

4. Supplementary Movies

Movie S1. Photoinduced right-handed helix (θ_1=40°, Film size: 20 mm×3 mm×25 μm) and photoinduced left-handed helix (θ_2=10°, Film size: 20 mm×3 mm×25 μm). The diameters of the helixes are related to the light intensities (composite **I**).

Movie S2. An asymmetric actuator (composite **I**) walking on different substrates.

Movie S3. Mimicking the predation of python, the prey is a metal plate (composite **I,** left-handed helix with θ_2=30°, Film size: 20 mm×3 mm×25 μm).

Movie S4. Mimicking the predation of python, the prey is a wood stick (composite **I,** left-handed helix with θ_2=30°, Film size: 20 mm×3 mm×25 μm).

Movie S5. Mimicking the python perching on tree (composite **I,** left-handed helix with θ_2=30°, Film size: 20 mm×3 mm×25 μm).

Movie S6. The explosive power of helical deformation (composite **I,** left-handed helix with θ_2=30°, Film size: 20 mm×3 mm×25 μm).

1 C. J. Barrett and O. M. Tanchak, *Macromolecules*, 2005, **38**, 10566.
2 Z. Cheng, S. Ma, Y. Zhang, S. Huang, Y. Chen and H. Yu, *Macromolecules*, 2017, **50**, 8317.
3 A. Teishev, S. Incardona, C. Migliaresi and G. Marom, *J. Appl. Polym. Sci.*, 1993, **50**, 503.
4 A. Lendlein and S. Kelch, *Angew. Chem. Int. Ed.*, 2002, **41**, 2034.
5 H. Zhou, C. Xue, P. Weis, Y. Suzuki, S. Huang, K. Koynov, G. K. Auernhammer, R. Berger, H.-J. Butt and S. Wu, *Nat. Chem.*, 2016, **9**, 145.